Coupled Free Vibrations of Liquid in a Three-Dimensional Rectangular Container with an Elastic Cover

Kang Ren, Guoxiong Wu and Yifeng Yang

View Online   Export Citation   CrossMark

Coupled Free Vibrations of Liquid in a Three-Dimensional Rectangular Container with an Elastic Cover

K. Ren,[1] G.X. Wu,[1, a)] and Y.F. Yang[1]

[1]Department of Mechanical Engineering, University College London, Torrington Place, London WC1E 7JE, United Kingdom

[a)]Corresponding author: G.X. Wu (g.wu@ucl.ac.uk)

Abstract

The coupled free vibration of liquid and its elastic cover, such as a plate or a membrane, in a three-dimensional rectangular tank is investigated through an analytical scheme based on velocity potential theory for the flow and the linear elastic theory for the cover. For the fluid domain, the velocity potential is expanded into double cosine series along the longitudinal and transverse direction respectively, with the corresponding eigenvalues determined from the impermeable conditions on the side walls. The vertical modes of the potential are obtained from the Laplace equation. The deflection of rectangular cover is expanded into the same double cosine series to match the potential, together with additional terms for satisfying the edge conditions. The polynomials are used for these additional terms which are then expanded into cosine series. For the expansions of the higher-order derivatives of the deflection, the derivatives of these polynomial terms are expanded into cosine series directly, rather than being obtained through differentiating the cosine series of the deflection, to avoid the non-convergent series. Through imposing the boundary conditions on the fluid-plate interface and edge conditions, an infinite matrix equation for the unknown coefficients can be established. The natural frequencies can be obtained when the determinant of the matrix is zero. In practical computation, the infinite matrix equation is truncated into finite size. Results are first provided for natural frequencies. This is followed by the corresponding natural mode shapes and principal strains distribution on the cover. The underlying physics of these results are then provided.

Key words: fluid/structure interaction; rectangular tank; natural modes; liquid sloshing; elastic cover; eigenfunction expansions.

1. Introduction

The motion of liquid inside a tank or container, which is also named as sloshing, has received extensive study as it can be commonly seen in nature and has a wide range of engineering applications. Sloshing may occur in lakes, reservoirs, harbours, and bays, referred to as seiches[1], due to some environmental excitation such as winds and earthquakes. In marine engineering, sloshing can occur in a tank of a ship containing liquid, for example during its transportation of the liquified natural gas (LNG) and other types of liquid fuels such as liquid hydrogen (LH$_2$). Violent motion of liquid inside the tank can be excited by the motion of the ship, especially when the oscillation frequency of the ship is close to one of the natural frequencies of the tank. This may have severe adverse effect on the ship stability, also induce large impact loads and cause structural damage to the tank. On the other hand, sloshing can be used beneficially through anti-rolling tanks installed in ships to provide a moment to counter that due to wave excitation[2]. In addition, during transportation of liquefied fuels by ships or trucks, one of the main challenges is the potential boil-off which can be caused through evaporation of liquid fuels. Excessive boil-off gas may influence the operating pressure in the container and risk the safe transportation. The liquid sloshing in tanks can affect the rate of boil-off through the heat and mass transfer between liquid and vapor[3]. There are many other areas where sloshing can be important. For example, sloshing also occurs in the liquid-propellant container of spacecraft[4] and aircraft[5], in the fuel tank of other vehicles such as automobiles[6]. Furthermore, tuned liquid dampers (TLD) have been widely used in high-rise buildings to dampen the wind-induced vibration[7].

The literature on free surface sloshing modelling based on different governing equations such as the Navier-Stokes (NS) equations and Laplace equation have been summarized in Ibrahim[8] and Faltinsen and Timokha[9]. In particular, there is an extensive amount of work on free surface sloshing in a three-dimensional (3D) rectangular tank due to the practical importance. Based on the velocity potential flow theory, an analytical solution for small amplitude motions was given by Abramson[10]. For large amplitude motions, Wu et al.[11] developed a fully nonlinear finite element method and obtained the solution

62   numerically, and Faltinsen et al.[12] obtained the solutions based on the multimodal

63   approach. Based on the viscous theory, one of the examples is that by Liu and Lin[13],

64   where NS equations were solved numerically together with the large eddy simulation,

65   and volume of fluid method was used to track the interface of liquid and air. Apart from

66   numerical simulation, experimental studies have also been widely undertaken for liquid

67   sloshing in tanks, such as Caron et al.[14] for a circular cylindrical tank, Núñez Aedo et

68   al.[15] for a rectangular tank and Zhang et al.[16] for a floating rectangular tank in water

69   waves.

70

71   Resonant sloshing in a container occurs when the excitation frequency is close to one

72   of the natural frequencies of the tank. When damping is also small, resonant motion can

73   be exceedingly large. In many cases, a tank can be characterised as a clean tank, and

74   the viscous damping is small[9]. Therefore, one of the optimal sloshing suppression

75   strategies is to shift the natural frequencies of the tank away from the range of excitation

76   frequencies. Structures such as baffles and elastic floating covers are commonly

77   designed and installed in containers. For example, a recent work done by Kuznetsov &

78   Motygin[17] considered the effect of radial baffles to the liquid sloshing in an upright

79   circular container. In addition, active sloshing control has also been proposed based on

80   these structures, such as in Hernández and Santamarina[18], Hasheminejad et al.[19], and

81   Xie and Zhao[20]. Among many options, one of them is to use an elastic thin cover on the

82   liquid surface. Thus, understanding of the effect of the elastic cover on sloshing is of

83   important practical relevance. The cover may be an elastic membrane and elastic plate.

84   Bauer[21] considered the free vibration of liquid in a circular tank completely covered by

85   an elastic membrane or plate based on the Bessel-Fourier series expansion. A 2D

86   rectangular tank with membrane cover was considered by Parasil & Watanabe[22], where

87   the effect of nonlinearity was included. Using a similar method as in Bauer[21], Bauer and

88   Komatsu[23] further investigated a circular tank covered by a doughnut-shaped elastic

89   plate which covers the liquid surface partially, with the inner circular area of the liquid

90   surface being free. The problem was reconsidered by Kim and Lee[24] using the Rayleigh-

91   Ritz method. For the case where a circular plate concentrically covers the free liquid

92   surface, while the outer liquid surface of a circular cylindrical container remains free,

93   Amabili[25] obtained the frequencies of the free vibration by using the Rayleigh-Ritz

94   method. Recently, Ren et al.[26] developed two different efficient methods for the circular

95   tank. Various edge conditions were considered. Extensive results were provided for

96   natural frequencies, modal shapes, and maximum principal strain. A related problem of

97   sloshing in cylindrical storage tanks under seismic excitation was considered by

98   Matsui[27].

99

100   The works mentioned above are all a circular tank with an elastic cover. There is little

101   work on a rectangular tank based on analytical or semi-analytical procedure. This will

102   therefore be considered in the present work. The free vibration of the coupled system

103   of liquid and an elastic cover will be studied through an analytical scheme based on the

104   linearized velocity potential flow theory and Kirchhoff-Love thin plate theory. It is

105   worth mentioning here that different from the free surface sloshing, some additional

106   challenges exist in this coupled fluid-plate problem. One is the higher-order derivative

107   term in the dynamic condition of the elastic plate, and another one is due to the treatment

108   of various edge conditions. In this work, an analytical scheme applicable for various

109   edge conditions has been developed, which allows us to investigate their influence in a

110   much more convenient way. It should be mentioned that the present problem and

111   scheme are very much different from those of a circular tank. Physically for the circular

112   tank, there is no coupling among different circumferential modes in commonly adopted

113   edge conditions, or, clamped, fixed and free. For the rectangular tank, the modes are

114   usually coupled. Mathematically, as the solutions in both cases are based on analytical

115   procedure, the method and derivation are very different. An obvious difference is that

116   in the horizontal plane one is done in the polar coordinate system, while the other is

117   done in the Cartesian coordinate system. More importantly, for the circular tank, both

118   the potential and the cover deflection are expanded into Fourier and Bessel series. The

119   expansions of the cover deflection and its derivatives are linked through integration by

120   parts. However, this method cannot be used for the rectangular plate and thus a different

121   method is used. The potential is expanded into cosine series in the horizontal directions.

122 The cover deflection is expanded similarly. To meet the edge conditions, four additional
123 terms are introduced in each direction in the cover deflection. Without loss of generality,
124 polynomial functions are used. For the circular tank, the natural frequencies can be
125 obtained from the roots of an infinite summation which is truncated. For the rectangular
126 tank, they are obtained when the determinant of an infinite matrix is zero, which is
127 truncated at a sufficiently large number. However, when the size of the matrix increases,
128 direct computation of the determinant becomes impractical. A Gaussian elimination
129 scheme is then used to search for the natural frequencies. Extensive results are provided
130 for natural frequencies, mode shapes and maximum principal strain.

131

132 The paper is organized as follows. In Section 2, the mathematical model and solution
133 procedure are introduced. Detailed results and discussion on the natural frequencies,
134 mode shapes and principal strain are respectively provided in Sections 3, 4 and 5.
135 Finally, conclusions are drawn in Section 6.

136

2. Mathematical model and solution procedures

138 We consider the problem of free sloshing motion of liquid in a three-dimensional
139 rectangular tank of rigid side walls with an elastic cover. The sketch of this problem is
140 shown in Fig. 1. A fixed Cartesian coordinate system is established on the tank with the
141 origin located on the centre point of the undisturbed plane of the cover, with its z-axis
142 pointing vertically upward. The half length and width of the tank are denoted as l and
143 b, with their directions along the x- and y-axes, respectively. The depth of the liquid is
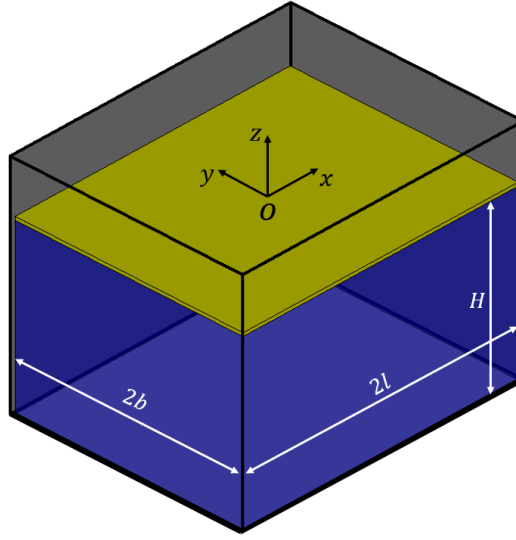144 H.

FIG. 1. The sketch of the problem

The velocity potential theory is adopted for fluid motion while the Kirchhoff-Love plate theory is adopted for the elastic cover in the mathematical modelling. Based on the assumption that the liquid in the tank is incompressible, the velocity potential Φ satisfies the Laplace equation

$$\frac{\partial^2 \Phi}{\partial x^2} + \frac{\partial^2 \Phi}{\partial y^2} + \frac{\partial^2 \Phi}{\partial z^2} = 0. \tag{1}$$

We assume that there is no gap between fluid and the elastic cover. The dynamic condition on the interface of liquid domain and elastic plate can be given as

$$\rho_e h \frac{\partial^2 W}{\partial t^2} + L\nabla^4 W = -\rho\Phi_t - \rho g W \qquad (z = 0), \tag{2}$$

where W is the deflection of the elastic plate, t is time, ρ is the density of liquid, g is the gravitational acceleration, and $L = Eh^3/[12(1-v^2)]$, E, h, ρ_e and v are respectively the flexural rigidity, Young's modulus, thickness, density and Poisson's ratio of the plate. $\nabla^4 = \nabla^2\nabla^2$ is the biharmonic differential operator. The right-hand side of Eq. (2) is the fluid pressure acting on the elastic cover, which is obtained from linearized Bernoulli equation. For a membrane, the term of $L\nabla^4 W$ in Eq. (2) should be replaced by $T\nabla^2 W$, where T is the tension. Without loss of generality, the derivation and results below will focus on the plate.

164

165   The linearized kinematic condition at the interface can be given as

$$\frac{\partial W}{\partial t} = \frac{\partial \Phi}{\partial z}, \qquad (z = 0). \tag{3}$$

167   On the rigid side walls and bottom of the tank, we have the impermeable boundary

168   conditions as

$$\left.\frac{\partial \Phi}{\partial x}\right|_{x=\pm l} = \left.\frac{\partial \Phi}{\partial y}\right|_{y=\pm b} = \left.\frac{\partial \Phi}{\partial z}\right|_{z=-H} = 0. \tag{4}$$

170   In addition, the boundary conditions for plate edges must be imposed. The most

171   commonly used types are clamped, free and simply supported edges. On the edge of

172     $x = \pm l$, we have

$$W(x = \pm l) = 0, \qquad W_x(x = \pm l) = 0, \tag{5a, b}$$

174   for clamped edge,

$$\left(\frac{\partial^2 W}{\partial x^2} + v\frac{\partial^2 W}{\partial y^2}\right)_{x=\pm l} = 0, \qquad \left(\frac{\partial^3 W}{\partial x^3} + (2-v)\frac{\partial^3 W}{\partial x \partial y^2}\right)_{x=\pm l} = 0, \tag{6a, b}$$

176   for free edge, and

$$W(x = \pm l) = 0, \qquad \left(\frac{\partial^2 W}{\partial x^2} + v\frac{\partial^2 W}{\partial y^2}\right)_{x=\pm l} = 0, \tag{7a, b}$$

178   for simply supported edge[29]. For the other pair of edges at $y = \pm b$, the corresponding

179   equations for the edge conditions can be obtained from Eqs. (5) to (7) by simply

180   exchanging x and y. For the free corner formed by two free edges, the condition $\frac{\partial^2 w}{\partial x \partial y} =$

181   0 should be also satisfied[29,30].

182

183   To investigate the free vibration of the system, we may write $\Phi = \mathrm{Re}\{\phi \times e^{-i\omega t}\}$ and

184     $W = \mathrm{Re}\{w \times e^{-i\omega t}\}$, where ω is a natural frequency of the system, and $i = \sqrt{-1}$ is the

185   imaginary unit. Taking into account Eq. (4), expanding ϕ into cosine series in x and y

186 directions, and then solving ordinary differential equation in the z direction, we can

187 write the solution of ϕ as

$$\phi = \sum_{m=0}^{\infty} \sum_{n=0}^{\infty} \mathcal{P}_{mn} \cos a_m(x+l) \cos b_n(y+b) \frac{\cosh k_{mn}(z+H)}{\cosh k_{mn}H} \tag{8}$$

189 where

$$a_m = \frac{m\pi}{2l}, \qquad b_n = \frac{n\pi}{2b}, \qquad k_{mn}^2 = a_m^2 + b_n^2. \tag{}$$

190

191

192 By substituting Eq. (8) into the dynamic equation of plate, we have

$$L\nabla^4 w + (\rho g - \rho_e h\omega^2)w = i\rho\omega \sum_{n=0}^{\infty} \sum_{m=0}^{\infty} \mathcal{P}_{mn} \cos a_m(x+l) \cos b_n(y+b). \tag{9}$$

194 The solution of w may be written as

$$w = w_0 + w_1 + w_2. \tag{10}$$

196 Here, w_0 can be written in the form of double series given the right-hand side of Eq. (9)

$$w_0 = \sum_{n=0}^{\infty} \sum_{m=0}^{\infty} C_{mn} \cos a_m(x+l) \cos b_n(y+b), \tag{11}$$

198 and w_1 and w_2 in Eq. (10) are introduced to account for edge conditions at $x = \pm l$

199 and $y = \pm b$, respectively. We may write w_1 in the following form

$$w_1 = \sum_{n=0}^{\infty} \cos b_n(y+b) \cdot f_n(x). \tag{12}$$

201 We notice that the edge conditions in Eqs. (5) to (7) have two conditions on each side

202 and four in total, involving derivatives up to third order. Taking this account, we may

203 write

$$f_n(x) = d_n^{(1)}\left(\frac{x}{l}\right) + d_n^{(2)}\left(\frac{x}{l}\right)^2 + d_n^{(3)}\left(\frac{x}{l}\right)^3 + d_n^{(4)}\left(\frac{x}{l}\right)^4. \tag{13}$$

205 Similarly, we may write w_2 as

206
$$w_2 = \sum_{m=0}^{\infty} \cos a_m(x + l) \cdot g_m(y), \tag{14}$$

207 with

208
$$g_m(y) = c_m^{(1)}\left(\frac{y}{b}\right) + c_m^{(2)}\left(\frac{y}{b}\right)^2 + c_m^{(3)}\left(\frac{y}{b}\right)^3 + c_m^{(4)}\left(\frac{y}{b}\right)^4. \tag{15}$$

209 In this way, the satisfaction of the governing equation is taken care of by C_{mn} in Eq.

210 (11), edge conditions at $x = \pm l$ by $d_n^{(i)}$, $i = 1,2,3,4$ in Eq. (13), and edge conditions by

211 $c_m^{(i)}$, $i = 1,2,3,4$ in Eq. (15), while they are all coupled. Then, w can then be written as

212
$$w = \sum_{n=0}^{\infty}\sum_{m=0}^{\infty} C_{mn} \times \cos a_m(x + l)\cos b_n(y + b) + \sum_{n=0}^{\infty} \cos b_n(y + b) \cdot f_n(x)$$

213
$$+ \sum_{m=0}^{\infty} \cos a_m(x + l) \cdot g_m(y). \tag{16}$$

214 Here we may notice that w in Eq. (16) is similar to that in Li et al.[31] for a plate without

215 liquid, where a different procedure is followed.

216

217 We may expand $\left(\frac{x}{l}\right)^i$ and $\left(\frac{y}{b}\right)^i$ ($i = 0\sim4$) into following series

218
$$\left(\frac{x}{l}\right)^i = \sum_{m=0}^{\infty} \mu_m^{(i)} \cos a_m(x + l), \tag{17}$$

219
$$\left(\frac{y}{b}\right)^i = \sum_{n=0}^{\infty} \mu_n^{(i)} \cos b_n(y + b), \tag{18}$$

220 where $\mu_n^{(0)} = \delta_{n0}$ and

221
$$\mu_n^{(1)} = \begin{cases} 0, & n = 0 \\ \dfrac{4(-1 + (-1)^n)}{n^2\pi^2}, & n > 0 \end{cases};$$

222
$$\mu_n^{(2)} = \begin{cases} 1/3, & n = 0 \\ \dfrac{8(1 + (-1)^n)}{n^2\pi^2}, & n > 0 \end{cases};$$

9

223

$$\mu_n^{(3)} = \begin{cases} 0, & n = 0 \\ \dfrac{12(n^2\pi^2 - 8)(-1 + (-1)^n)}{n^4\pi^4}, & n > 0 \end{cases} ;$$

224

$$\mu_n^{(4)} = \begin{cases} 1/5, & n = 0 \\ \dfrac{16(n^2\pi^2 - 24)(1 + (-1)^n)}{n^4\pi^4}, & n > 0 \end{cases} .$$

225

226   Substituting Eqs. (16), (17) and (18) into (9), then based on the orthogonality of the

227   trigonometric functions, we have

228
$$\sum_{i=1}^{4} \left(\alpha_{mn}^{(i)} c_m^{(i)} + \beta_{mn}^{(i)} d_n^{(i)} \right) = S_{mn} C_{mn} + i\rho\omega\mathcal{P}_{mn} \quad (m,n = 0,1,2,3,\dots), \quad (19)$$

229   where

230   $S_{mn} = -[L(a_m^2 + b_n^2)^2 + \rho g - \rho_e h \omega^2],$ \hfill (20)

231   $\alpha_{mn}^{(i)} = (La_m^4 + \rho g - \rho_e h\omega^2)\mu_n^{(i)} - \dfrac{4La_m^2}{b^2}\delta_{n0}\delta_{i2} - \dfrac{12La_m^2}{b^2}\mu_n^{(1)}\delta_{i3}$

232   $\qquad\qquad + \left(\dfrac{24L}{b^4}\delta_{n0} - \dfrac{24La_m^2}{b^2}\mu_n^{(2)} \right)\delta_{i4}$

233   $\qquad\qquad = -S_{m0}\mu_n^{(i)} + \dfrac{24L}{b^4}\delta_{n0}\delta_{i4} - \dfrac{2a_m^2 L \times i(i-1)\,\mu_n^{(i-2)}}{b^2},$ \hfill (21)

234   $\beta_{mn}^{(i)} = (Lb_n^4 + \rho g - \rho_e h\omega^2)\mu_m^{(i)} - \dfrac{4Lb_n^2}{l^2}\delta_{m0}\delta_{i2} - \dfrac{12Lb_n^2}{l^2}\mu_m^{(1)}\delta_{i3}$

235   $\qquad\qquad + \left(\dfrac{24L}{l^4}\delta_{m0} - \dfrac{24Lb_n^2}{l^2}\mu_m^{(2)} \right)\delta_{i4}$

236   $\qquad\qquad = -S_{0n}\mu_m^{(i)} + \dfrac{24L}{l^4}\delta_{m0}\delta_{i4} - \dfrac{2b_n^2 L \times i(i-1)\,\mu_m^{(i-2)}}{l^2},$ \hfill (22)

237   and δ_{ij} is the Kronecker delta function.

238

239   Here we may notice that the expansions of the derivatives of $f(x)$ and $g(y)$ are

240   obtained respectively from Eqs. (17) and (18) directly, rather than from the derivatives

241   of their expansions, as the latter may lead to a non-convergent series.

242

10

243   The kinematic condition is

244
$$-\mathrm{i}\omega w = \phi_z, \quad z = 0. \tag{23}$$

245   Substituting Eqs. (8), (13), (15), (16) into Eq. (23), and further based on the

246   orthogonality of trigonometric functions, we have

247
$$-\mathrm{i}\omega\left(\sum_{i=1}^{4}\mu_m^{(i)}d_n^{(i)} + \sum_{i=1}^{4}\mu_n^{(i)}c_m^{(i)}\right) = k_{mn}\tanh k_{mn}H \ \mathcal{P}_{mn} + \mathrm{i}\omega C_{mn}.$$

248
$$(m,n = 0,1,2,3\ldots) \tag{24}$$

249   From Eqs. (19) and (24), we can write $\mathcal{P}_{mn}$ and C_{mn} in terms of $c_m^{(i)}$ and $d_n^{(i)}$ as

250
$$\mathcal{P}_{mn} = -\frac{\mathrm{i}\omega}{k_{mn}S_{mn}\tanh k_{mn}H + \rho\omega^2}$$

251
$$\times \sum_{i=1}^{4}\left[\left(S_{mn}\mu_m^{(i)} + \beta_{mn}^{(i)}\right)d_n^{(i)} + \left(S_{mn}\mu_n^{(i)} + \alpha_{mn}^{(i)}\right)c_m^{(i)}\right], \tag{25}$$

252
$$C_{mn} = -\frac{\rho\omega^2}{S_{mn}(k_{mn}S_{mn}\tanh k_{mn}H + \rho\omega^2)}$$

253
$$\times \sum_{i=1}^{4}\left[\left(S_{mn}\mu_m^{(i)} + \beta_{mn}^{(i)}\right)d_n^{(i)} + \left(S_{mn}\mu_n^{(i)} + \alpha_{mn}^{(i)}\right)c_m^{(i)}\right]$$

254
$$+\frac{1}{S_{mn}}\sum_{i=1}^{4}\left(\alpha_{mn}^{(i)}c_m^{(i)} + \beta_{mn}^{(i)}d_n^{(i)}\right). \qquad (m,n = 0,1,2,3\ldots) \tag{26}$$

255   Apart from Eqs. (19) and (24), edge conditions also need to be imposed on w in Eq.

256   (16). By using orthogonality of trigonometric functions and substituting the expressions

257   of $\mathcal{P}_{mn}$ and C_{mn} in Eqs. (25) and (26), we can obtain systems of linear equations for

258   unknowns $c_m^{(i)}$ and $d_n^{(i)}$ shown in various edge conditions of appendices. The matrix

259   equation can be written as

260
$$\boldsymbol{A}\cdot\boldsymbol{x} = \boldsymbol{0}, \tag{27}$$

261   where $\boldsymbol{x}$ is a column vector which can be written as

262
$$\boldsymbol{x} = [\boldsymbol{c_0}, \boldsymbol{c_1}, \ldots, \boldsymbol{c_m}, \ldots, \boldsymbol{d_0}, \boldsymbol{d_1}, \ldots, \boldsymbol{d_n}, \ldots]^T,$$

11

263   with $\boldsymbol{c}_m = \left(c_m^{(1)}, c_m^{(2)}, c_m^{(3)}, c_m^{(4)}\right)$ and $\boldsymbol{d}_n = \left(d_n^{(1)}, d_n^{(2)}, d_n^{(3)}, d_n^{(4)}\right)$. The coefficients of

264   matrix $\boldsymbol{A}$ in Eq. (27) can be obtained from individual equations in the appendices for

265   each set of edge conditions. In practical calculation, truncations are made for m and n

266   at $M - 1$ and $N - 1$, respectively.

267

268   The natural frequencies correspond to the roots of $\det\{\boldsymbol{A}\} = 0$, or the values of ω^* at

269   which the coefficient matrix is singular. As the size of matrix increases, direct

270   computation of its determinant becomes impractical. To search for the roots of

271   $\det\{\boldsymbol{A}\} = 0$, we vary ω^* with a sufficiently small interval $\Delta\omega^*$. We then use the

272   Gaussian elimination algorithm with column pivoting. When the Gaussian elimination

273   reaches the kth row, column swapping is conducted to ensure the diagonal element to

274   be the principal one. When the absolute value of the principal element is sufficiently

275   small or is below a given small threshold value, then the matrix is regarded to be

276   singular. To reduce the computational cost, we may investigate $\det\{\boldsymbol{A}\} = 0$ directly for

277   smaller M and N, which can give a good estimate for the positions of the solutions.

278   Then, we can further use the Gaussian elimination near these points at larger M and N.

279

280   For cases with edge conditions of the same type on the four edges, we can further split

281   the unknowns $\boldsymbol{x}$ in Eq. (27) into four groups: (a). $c_{2m}^{(2i)}, d_{2n}^{(2i)}$; (b). $c_{2m}^{(2i-1)}, d_{2n+1}^{(2i)}$; (c).

282   $c_{2m+1}^{(2i)}, d_{2n}^{(2i-1)}$; and (d). $c_{2m+1}^{(2i-1)}, d_{2n+1}^{(2i-1)}$ $(i = 1,2; m, n = 0,1,2 \ldots)$, which respectively

283   correspond to the symmetric-symmetric (S-S) modes, the symmetric-antisymmetric (S-

284   A) modes, the antisymmetric-symmetric (A-S) modes and the antisymmetric-

285   antisymmetric (A-A) modes with respect to x and y axes. The detailed analysis for

286   completely clamped edges can be seen in appendix A, while the other two sets of edge

287   conditions can be analysed in a similar way. Therefore, the unknowns in each group are

288   coupled with each other but are fully uncoupled with those in other three groups. In

289   such cases, the natural frequencies in each group can be obtained from the solutions of

290   the zero-determinant of the matrix corresponding to this group. For a square tank, it can

291   be expected that the natural frequencies of the A-S mode are the same as those of S-A

292   modes.

293

294   The free corner condition $w_{xy} = 0$ is satisfied automatically by in the present procedure.

295   Integrate the zero Kirchhoff shear force edge condition at $x = -l$ in Eq. (6) with respect

296   to y from $-b$ to b, we have

297
$$\int_{-b}^{b} \left[\frac{\partial^3 w}{\partial x^3} + (2 - v) \frac{\partial^3 w}{\partial x \partial y^2} \right]_{x=-l} dy$$

298
$$= \int_{-b}^{b} \frac{\partial^3 w}{\partial x^3} \bigg|_{x=-l} dy + (2 - v) \left[\frac{\partial^2 w}{\partial x \partial y} \bigg|_{x=-l,y=b} - \frac{\partial^2 w}{\partial x \partial y} \bigg|_{x=-l,y=-b} \right] = 0$$

299   (28)

300   Using Eq. (10) for w_{xxx} with f_n''' being obtained directly from Eq. (13), and then (B.5)

301   for $n = 0$, we obtain

302
$$\frac{\partial^2 w}{\partial x \partial y} \bigg|_{x=-l,y=b} - \frac{\partial^2 w}{\partial x \partial y} \bigg|_{x=-l,y=-b} = -\frac{2b}{2-v} \times f_0'''(-l) = -\frac{2b\left(6d_0^{(3)} - 24d_0^{(4)}\right)}{(2-v)l^3} = 0$$

303   (29)

304   In addition, multiply Eq. (6a) by $\cos b_1(y + b)$ first and then integrate as in Eq. (28).

305   Using integration by parts twice for the second term, we have

306
$$\int_{-b}^{b} \left[\frac{\partial^3 w}{\partial x^3} + (2 - v) \frac{\partial^3 w}{\partial x \partial y^2} \right]_{x=-l} \cos b_1(y + b) \, dy$$

307
$$= b f_1'''(-l) + (2 - v) \left\{ \left[\cos b_1(y + b) \left(\frac{\partial^2 w}{\partial x \partial y} \right)_{x=-l} \right]_{-b}^{b} - b b_1^2 f_1'(-l) \right\} = 0,$$

308   (30)

309   or

310 $[w_{xy}]_{x=-l,y=b} + [w_{xy}]_{x=-l,y=-b} = \dfrac{b}{2-v} \times [f_1'''(-l) - (2-v)b_1^2 f_1'(-l)]$

311 $= \dfrac{b}{2-v}\left[\dfrac{(2-v)b_1^2}{l}\left(-d_1^{(1)} + 2d_1^{(2)} - 3d_1^{(3)} + 4d_1^{(4)}\right) + \dfrac{6}{l^3}d_1^{(3)} - \dfrac{24}{l^3}d_1^{(4)}\right].$

312 $\hspace{11cm}(31)$

313 By using Eq. (B.5) for $n = 1$, we can further have $w_{xy}\big|_{x=-l,y=b} + w_{xy}\big|_{x=-l,y=-b} = 0$.

314 Therefore, we have $w_{xy}\big|_{x=-l,y=b} = w_{xy}\big|_{x=-l,y=-b} = 0$ when free edge conditions are

315 imposed in the appendix of the present procedure. Similar operation can be applied

316 other free edges, and therefore we have on all the four corners, or $w_{xy}\big|_{x=\pm l,y=\pm b} = 0$.

317

318 ## 3. Natural frequencies

319 ### 3.1 Natural frequencies of a rectangular plate without liquid

320 When there is no liquid beneath the elastic plate, the rectangular plate is vibrating in the

321 vacuum. In such a case, $\rho = 0$ can be taken in all the above equations. The solution may

322 be compared with existing results, such as those provided by Leissa[30], to verify the

323 present procedure. The threshold value used in the Gaussian elimination is chosen as

324 10^{-4}. In TABLE 1 to 3, we give the present results and those from Leissa[30] of the six

325 lowest natural frequencies at three different combinations of edge conditions on the four

326 edges, namely, completely clamped edges (*C-C-C-C*), completely free edges (*F-F-F-*

327 *F*), and one clamped, one simply supported and two neighbouring free edges (*C-SS-F-*

328 *F*). The case with aspect ratio $l/b = 1.5$ is used as an example.

329

330

331

332

333

334

TABLE 1. Natural frequency parameters ($\lambda = 4l^2\omega\sqrt{\rho_e h/L}$) for completely clamped edges (C-C-C-C), ($v = 0.3$).

frequency sequence	Leissa[30]	Present results		
		$M = N = 10$	$M = N = 15$	$M = N = 20$
1	60.772	60.757	60.761	60.761
2	93.860	93.821	93.831	93.833
3	148.82	148.76	148.78	148.78
4	149.74	149.64	149.67	149.67
5	179.66	179.51	179.55	179.56
6	226.92	226.78	226.81	226.82

TABLE 2. Natural frequency parameters ($\lambda = 4l^2\omega\sqrt{\rho_e h/L}$) for completely free edges (F-F-F-F), ($v = 0.3$).

frequency sequence	Leissa[30]	Present results		
		$M = N = 10$	$M = N = 15$	$M = N = 20$
1	20.128	20.101	20.097	20.096
2	21.603	21.431	21.417	21.415
3	46.654	46.393	46.358	46.352
4	50.293	49.952	49.919	49.915
5	58.201	57.814	57.748	57.726
6	67.494	67.096	67.050	67.038

TABLE 3. Natural frequency parameters ($\lambda = 4l^2\omega\sqrt{\rho_e h/L}$) for one clamped, one simply supported and two neighbouring free edges (C-SS-F-F), ($v = 0.3$).

frequency sequence	Leissa[30]	Present results		
		$M = N = 10$	$M = N = 15$	$M = N = 20$
1	6.9309	6.9094	6.9133	6.9148
2	27.289	27.142	27.159	27.166
3	38.586	38.391	38.384	38.384
4	64.254	63.985	64.001	64.011
5	67.467	67.227	67.194	67.188
6	108.02	107.70	107.69	107.70

In above tables, it can be observed that convergence with N and M has been achieved for the present results, especially the maximum relative error between results at $N = M = 15$ and $N = M = 20$ is smaller than 0.05%. A very good agreement between the present results and those in Leissa[30] can also be seen.

352   It may seem that by simply taking liquid density $\rho \to 0$ in the solution procedure in

353   Section 2 the result will be identical to that of $\rho = 0$, or the free vibration of a

354   rectangular plate in vacuum. However, as it can be seen in appendices the equations

355   may not reduce to those for rectangular plate in vacuum. In fact, we may consider the

356   term $\frac{k_{mn} \tanh k_{mn}H}{S_{mn}k_{mn}\tanh k_{mn}H + \rho\omega^2}$. At $m = n = 0$, this is always zero when ρ tends to zero but

357   is not equal to zero. It becomes non-zero when $\rho = 0$. This kind of difference may affect

358   the results of ω^*, which depends on the edge conditions. For *C-C-C-C* conditions, it is

359   noticed that some frequencies at $\rho \to 0$ are the same as those at $\rho = 0$ and others are

360   not. As $m = n = 0$ belongs to the S-S modes, only the natural frequencies

361   corresponding to S-S modes are affected while others are not. For *F-F-F-F* edge

362   conditions, as shown in (B1) to (B4) in appendix B, there is always a factor $(a_m^2 + \nu b_n^2)$

363   in the series which equals zero at $m = n = 0$. Therefore, the coefficient matrix will

364   always be the same for both $\rho \to 0$ and $\rho = 0$, so as the solutions of ω^*.

365

366   Physically, when $\rho \to 0$, the dynamic effect of the liquid on the plate will disappear, or

367   the right-hand side of Eq. (2) will be zero. However, the kinematic condition in Eq. (3)

368   remains. As the integration of the normal derivative of the potential, $\partial\phi/\partial n$, over the

369   fluid boundary must be zero due to mass continuity, or the Laplace equation, the

370   integration of the right-hand side of Eq. (3) over the plate must be zero because

371    $\partial\phi/\partial n = 0$ on all other boundaries. This means that the mean of the deflection w must

372   be zero. This condition is not always necessary or is not met for a plate in the vacuum.

373   Therefore, these two cases are not identical. Also, physically, when ρ is very small, the

374   liquid may not be treated as incompressible. If we include the compressibility effect at

375   small ρ, for example through the wave equation $\nabla^2\Phi - \Phi_{tt}/c^2 = 0$, where c is the

376   speed of sound in the liquid, then these two cases do become identical. In fact, by

377   substituting Eq. (8) into the wave equation, we can have $k_{mn}^2 = a_m^2 + b_n^2 - \omega^2/c^2$.

378   Then equations in appendices will become for plate in vacuum when $\rho \to 0$.

379

380

3.2 Natural frequencies of the coupled fluid-elasticity system

We now consider the case of liquid in the container with an elastic cover. The natural frequencies are calculated based on the solution procedures developed in Section 2. In the following calculation, dimensionless variables are used based on three characteristic variables, namely, the half-length l, the density of liquid ρ, and the acceleration due to gravity g. Based on their combinations, all parameters mentioned below are nondimensionalised with an asterisk as its superscript, or $b^* = b/l$, $H^* = H/l$, $m^* = \rho_e h/(\rho l)$, $L^* = L/(\rho g l^4)$ and $\omega^* = \omega\sqrt{l/g}$.

We consider the effect of different ratios of b/l on the natural frequencies at different edge conditions. The natural frequencies ω^* corresponding to different values of b^* are provided in TABLE 4 to 6 for completely clamped edges (*C-C-C-C*), completely free edges (*F-F-F-F*), and completely simply supported edges (*SS-SS-SS-SS*), respectively. They are arranged in the ascending order of ω^*. Further to the previous analysis, we have marked the group which each natural frequency belongs to in TABLE 4 to 6. The results for different combinations of these three conventional edge conditions can be obtained in a similar way.

For the free surface sloshing problem in a 3D rectangular tank, the modes at different m or n are fully uncoupled and natural frequencies can be easily obtained from $\omega_{mn}^2 = g k_{mn} \tanh(k_{mn}H)$, $m, n = 0,1,2 \ldots$ In general, $\omega_{mn} \neq \omega_{nm}$ when $n \neq m$. However, they become the same frequency when $l = b$. This means that swapping n and m, or swapping the wave patterns in x and y will give the same frequency. When there is a plate on the top of the liquid, the modes at different m and n are not fully uncoupled. However, swapping the patterns in the x and y directions of a square tank still give the same frequency if the edge conditions on four sides are same. Mathematically, in S-S and A-A groups discussed previously, c and d can be simply swapped. In A-S, when c and d are swapped, it becomes S-A. This means that we can swap the deflection

409   patterns in the x and y directions, and they give the same natural frequency, as can be

410   seen in the following tables.

411

412   In TABLE 4, we can observe that for each column corresponds to mode sequence i ($i =$

413     $1\sim6$), the natural frequencies will decrease as the increase of b^*. This is similar to the

414   trend of a rectangular plate in vacuum, shown in Table C1 in Leissa[30] for the same edge

415   condition. However, we may find for *F-F-F-F* and *SS-SS-SS-SS*, this trend may not be

416   followed in our results shown in TABLE 5 and 6. These are different from the

417   observation in Tables C15 and A1 in Leissa[30] for the same edge conditions where this

418   trend still remains for a rectangular plate in vacuum.

419

420   **TABLE 4. Natural frequencies ω^* at different b^* with completely clamped edges *C-C-C-C*.**

421     $(m^* = 0.001, L^* = 0.1, H^* = 1, \nu = 0.3)$

b^*	ω^*					
	1	2	3	4	5	6
1/2	16.0994(A-S)	28.6810(S-S)	43.9108(S-A)	47.7197(A-S)	52.6813(A-A)	67.5184(S-A)
2/3	11.8108(A-S)	22.3649(S-A)	23.1988(S-S)	30.2318(A-A)	41.7875(A-S)	43.7442(S-A)
1	9.1023(S-A)	9.1023(A-S)	16.2526(A-A)	18.4141(S-S)	21.5904(S-S)	28.4469(S-A)
3/2	4.1779(S-A)	8.0426(A-S)	8.4907(S-S)	10.9605(A-A)	15.1390(S-A)	15.9108(A-S)
2	2.6628(S-A)	5.1360(S-S)	7.6821(A-S)	8.4637(S-A)	9.2951(A-A)	11.9837(A-S)

422

423   **TABLE 5. Natural frequencies ω^* at different b^* with completely free edges *F-F-F-F*.**

424     $(m^* = 0.001, L^* = 0.1, H^* = 1, \nu = 0.3)$

b^*	ω^*					
	1	2	3	4	5	6
1/2	1.2002(A-S)	1.5010(A-S)	1.6934(S-A)	2.4870(A-S)	3.0521(A-A)	3.1625(S-S)
2/3	1.2010(A-S)	1.5037(A-S)	1.5076(S-A)	2.5184(A-S)	2.6080(A-A)	3.0194(S-A)
1	1.2022(S-A)	1.2022(A-S)	1.5079(S-A)	1.5079(A-S)	2.2786(A-A)	2.4421(A-A)
3/2	0.9059(S-A)	0.9537(S-A)	1.2032(A-S)	1.5116(A-S)	1.6891(A-A)	1.8050(S-S)
2	0.7197(S-A)	0.7302(S-A)	1.2038(A-S)	1.3170(S-S)	1.4693(A-A)	1.5081(S-S)

425

426   TABLE 6. Natural frequencies ω^* at different b^* with completely simply supported edges SS-SS-SS-SS.

427    $(m^* = 0.001, L^* = 0.1, H^* = 1, \nu = 0.3)$

b^*	ω^*					
	1	2	3	4	5	6
1/2	1.4977(S-A)	1.5060(A-A)	1.5218(S-S)	1.9596(A-S)	4.7899(S-S)	5.1958(S-A)
2/3	1.1241(A-A)	1.1493(S-A)	1.6721(S-S)	1.9572(A-S)	2.3616(S-A)	3.6550(A-A)
1	1.0193(A-A)	1.5558(S-S)	1.8619(A-A)	1.9808(S-A)	1.9808(A-S)	3.2982(A-A)
3/2	1.3514(S-A)	2.0377(A-S)	2.5319(A-A)	3.1297(S-S)	3.9334(A-S)	5.9092(S-A)
2	0.9216(S-A)	1.9329(A-S)	1.9905(S-S)	2.2986(A-A)	2.7888(A-S)	3.1103(S-A)

428

429   For the vibration of a completely simply supported plate (SS-SS-SS-SS) without fluid,

430   as the edge condition is symmetric about $y = 0$, it is expected to have both y-symmetric

431   and y-antisymmetric deflection modes at different natural frequencies. For the y-

432   antisymmetric modes, the corresponding natural frequencies will also be the natural

433   frequencies of a SS-SS-SS-SS plate with the same length l but half width $b/2$. This has

434   been pointed out in Leissa[30] and the reason provided is that a simply supported condition

435   is in fact satisfied along $y = 0$ in such a case. However, we find that it may be not

436   applicable here. From TABLE 6, we can find that there is no such a relationship between

437   results of $b^* = 1/2$ and $b^* = 1$, and results $b^* = 1$ and $b^* = 2$. This is of course due to

438   the coupling with of liquid and the side wall effects. For the y-antisymmetric case, for

439   the potential it is equivalent to the Dirichlet boundary condition $\phi = 0$ imposed on $y =$

440   0 which is different from the impermeable condition $\partial \phi / \partial n = 0$.

441

442   # 4. Mode shapes

443   Once natural frequencies have been determined, the corresponding natural mode shapes

444   can be further obtained. Using Eqs. (13), (15), (17) and (18), Eq. (16) yields

445
$$w(x,y) = \sum_{n=0}^{\infty} \sum_{m=0}^{\infty} I_{mn} \cos a_m(x + l) \cos b_n(y + b),   \tag{32}$$

446   where

19

447 $$I_{mn} = C_{mn} + \sum_{i=1}^{4} \mu_m^{(i)} d_n^{(i)} + \sum_{i=1}^{4} \mu_n^{(i)} c_m^{(i)}$$

448 $$= \sum_{i=1}^{4} \left(\beta_{mn}^{(i)} + \mu_m^{(i)} S_{mn} \right) T_{mn} d_n^{(i)} + \sum_{i=1}^{4} \left(\alpha_{mn}^{(i)} + \mu_n^{(i)} S_{mn} \right) T_{mn} c_m^{(i)},$$

449 $$(33)$$

450 and

451 $$T_{mn} = \frac{k_{mn} \tanh k_{mn} H}{k_{mn} S_{mn} \tanh k_{mn} H + \rho \omega^2}.$$

452 At a natural frequency, ω^*, when one of the non-zero deflection components $I_{m'n'}$ has

453 been prescribed, the other I_{mn} and the deflection w at each point (x, y) can be further

454 calculated. Specifically, for completely clamped, free or simply supported edge cases,

455 based on the natural mode groups (S-S, A-S, S-A, A-A) to which the natural frequency

456 belongs to, we may prescribe I_{02} (as I_{00} is always zero), I_{10}, I_{01} or I_{11} respectively to

457 work out other corresponding $I_{2m,2n}$, $I_{2m+1,2n}$, $I_{2m,2n+1}$ or $I_{2m+1,2n+1}$ terms, while the

458 remaining I_{mn} terms of other mode groups are zero. When the equation of prescribing

459 a particular I_{mn} becomes linearly dependent to the existing ones, we may also prescribe

460 $c_0^{(2)}$, $c_0^{(1)}$, $c_1^{(2)}$ and $c_1^{(1)}$ respectively for natural mode group S-S, A-S, S-A and A-A.

461

462 In Fig. 2, the normalized mode shapes, or $z^* = w^* / \max[w^*]$, corresponding to the first

463 six lowest natural frequencies are displayed for a square container covered by a clamped

464 square plate. Based on the previous analysis, we have also marked the natural mode

465 groups that the natural frequencies belong to. From the graphs, we can observe that the

466 mode shapes are consistent with what is expected for the symmetry and anti-symmetry

467 analysis. For a square tank, the S-A and A-S modes, such as displayed in Fig.2(a) and

468 2(b), have the same natural frequencies and their mode shapes become identical by

469 rotating one of them 90 degrees in the clockwise or counter-clockwise direction. In

470 addition, for different natural modes in the same mode group such as S-A, by comparing

471 Fig. 2(a) and 2(f), we can obverse that the mode shape becomes more complex with the

472 increase of the natural frequency. This is consistent with the observation in Ren et al.[26]

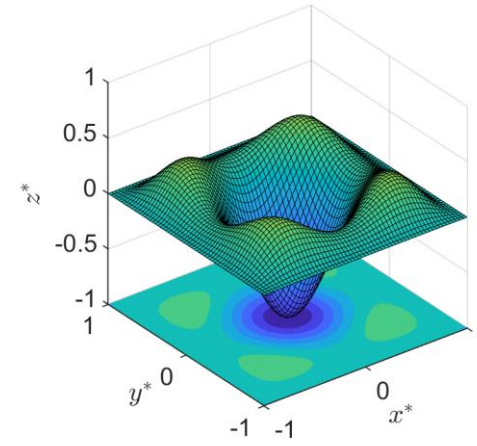473 for a circular tank, where further discussion has been provided.

474

475   (a)   (b)

476

477   (c)   (d)

478

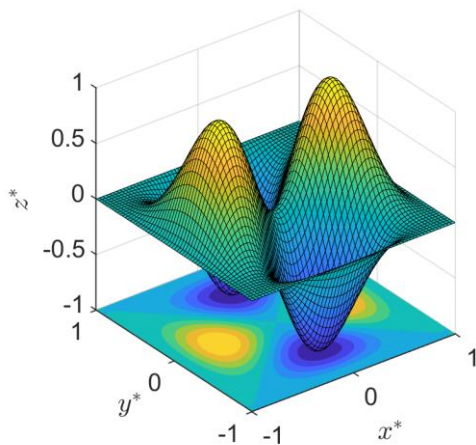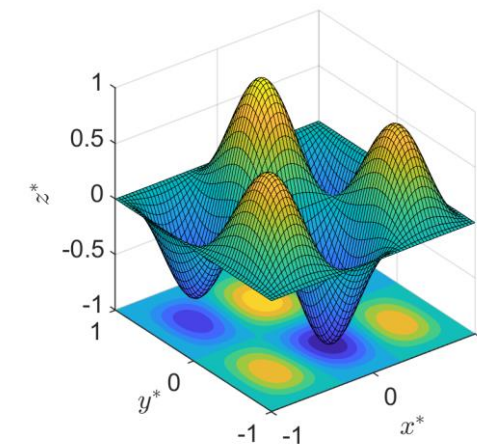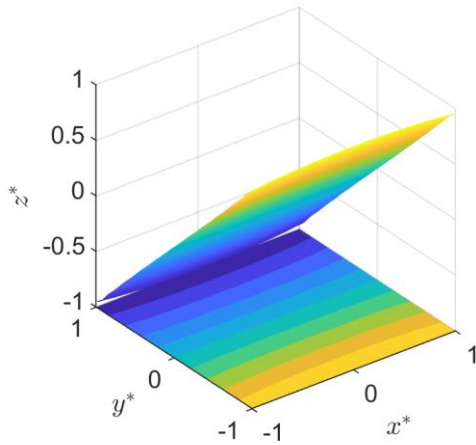479   (e)   (f)
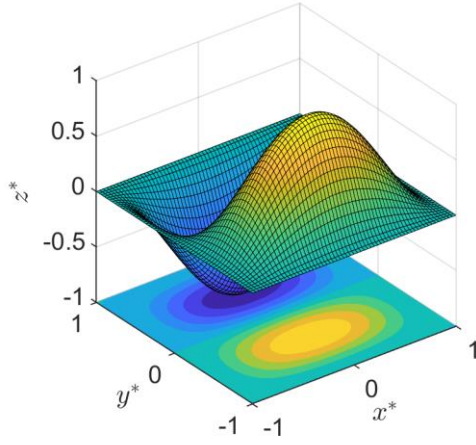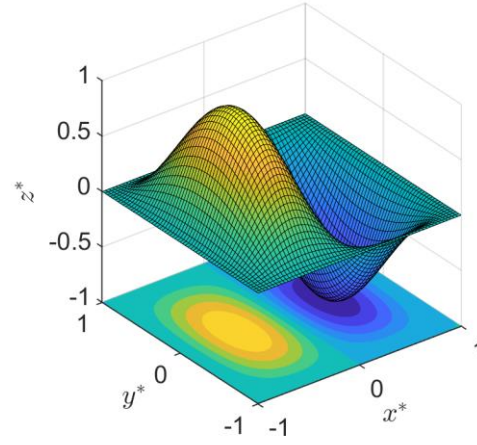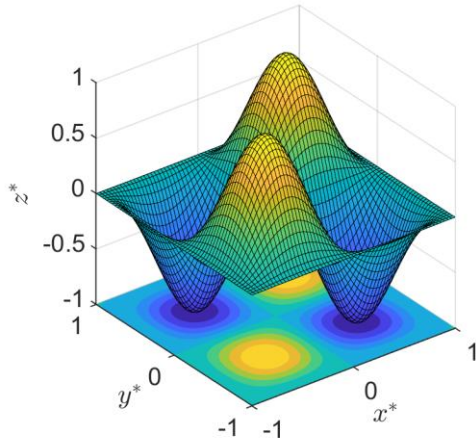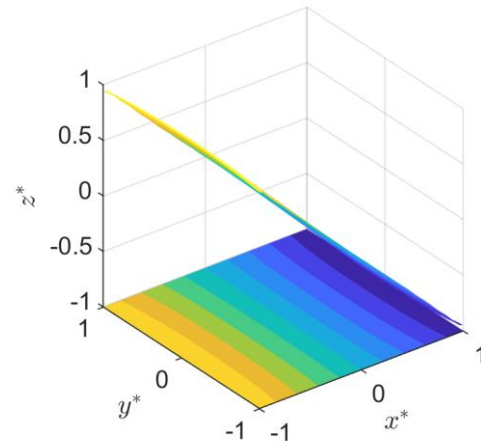
480   **FIG. 2.** Normalized mode shapes with clamped edges (C-C-C-C) in a square tank: $b^* = 1, m^* =$
481   $0.001, L^* = 0.1, H^* = 1, \nu = 0.3$. (a). $\omega^* = 9.1023$ (S-A); (b). $\omega^* = 9.1023$ (A-S); (c). $\omega^* =$
482   16.2526 (A-A); (d). $\omega^* = 18.4141$ (S-S); (e). $\omega^* = 21.5904$ (S-S); (f). $\omega^* = 28.4469$ (S-A).

483

484 Similarly, we display the normalized mode shapes of the first six lowest natural

485 frequencies of free edges (F-F-F-F) in Fig. 3. As there is no condition imposed on the

486 deflection and slope at the edges, the mode shapes are expected to be quite different

487 from those for clamped edges shown in Fig. 2. We can observe that the two mode shapes

488 shown in Fig. 3(a) and 3(b) belong to S-A and A-S modes respectively, which

489 correspond to a same natural frequency as explained previously. Similar pattern is also

490 shown in Fig. 3(c) and 3(d). However, major differences exist in the shape patterns

491 shown in Fig. 3(a) and Fig. 3(c). For example, the mode shapes in Fig. 3(c) and Fig.

492 3(d) are more curved than those in Fig. 3(a) and Fig. 3(b). Numerical results also show

493 that different from Fig. 3(c) and Fig. 3(d) where the maxima of the deflection are located

494 at the corners, in Fig. 3(a) and Fig. 3(b) they are located respectively at the middle of

495 the edges. Besides, the mode shapes shown in Fig. 3(e) and Fig. 3(f) are all A-A modes,

496 and the two corresponding nodal lines (where deflection is always zero during the

497 vibration) are all straight ones along the x- and y-axes. This can be also observed from

498 the result of I_{mn}. Based on the previous analysis, in A-A modes, only $I_{2m+1,2n+1}$ may

499 not be zero, and then as $\cos(2m+1)\pi/2 = 0$ and $\cos(2n+1)\pi/2 = 0$, it gives

500 $w(0,y) = w(x,0) = 0$.

501

502

503   (a)   (b)

504

505

506

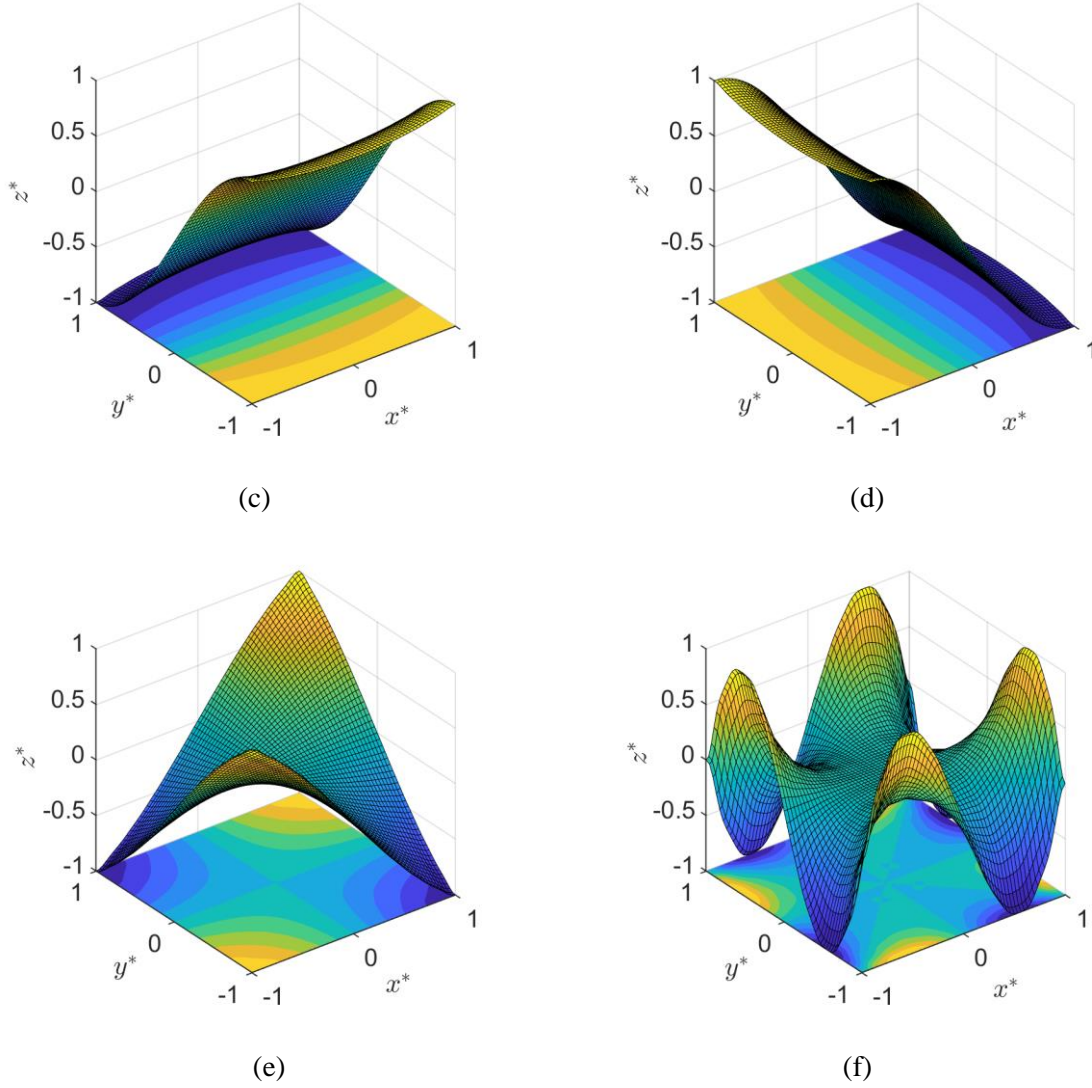507 (c)   (d)

508

509 (e)   (f)

510 **FIG. 3.** Normalized mode shapes with completely free edges in a square tank: $b^* = 1, m^* =$
511 $0.001, L^* = 0.1, H^* = 1, \nu = 0.3$. (a). $\omega^* = 1.2022$ (S-A); (b). $\omega^* = 1.2022$ (A-S); (c). $\omega^* = 1.5079$
512 (S-A); (d). $\omega^* = 1.5079$ (A-S); (e). $\omega^* = 2.2786$ (A-A); (f). $\omega^* = 2.4421$ (A-A).

513

514   In addition, for a square tank covered by a plate of the same edge conditions, it is also

515   observed that some mode shapes have symmetry or anti-symmetry feature with respect

516   to the diagonal line. For example, both Fig 3(e) and 3(f) belong to A-A mode group, but

517   are diagonally symmetric, or $w(-y, -x) = w(x, y)$, and anti-symmetric, or

518     $w(-y, -x) = -w(x, y)$, respectively. This can also be seen from the result of

519     $I_{2m+1,2n+1}$ $(m, n = 0,1,2, \dots)$. $I_{2m+1,2n+1} = I_{2n+1,2m+1}$ $(c_n = d_n, n = 0,1,2 \dots)$ gives

520   diagonally symmetric modes, while $I_{2m+1,2n+1} = -I_{2n+1,2m+1}$ $(c_n = -d_n, n =$

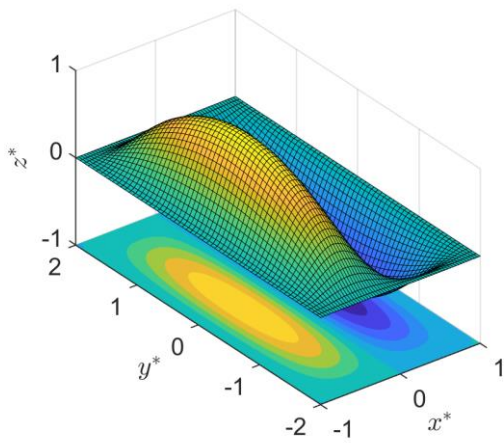521 $0,1,2 \dots)$ gives diagonally anti-symmetric modes. When $b \neq l$, the mode shapes are

23

522   shown in Fig. 4 for a plate with completely clamped edges (C-C-C-C). There is no

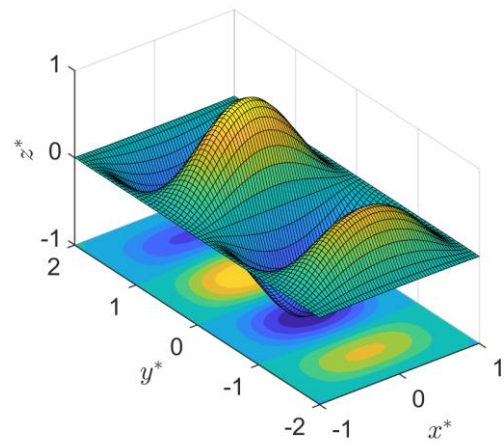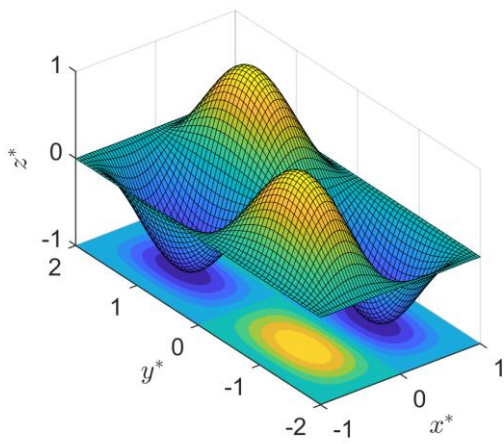523   longer diagonal symmetry or anti-symmetry.

524

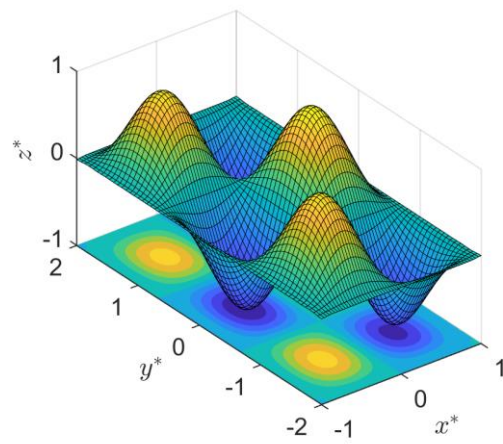525   (a)   (b)

526

527   (c)   (d)

528

529   (e)   (f)
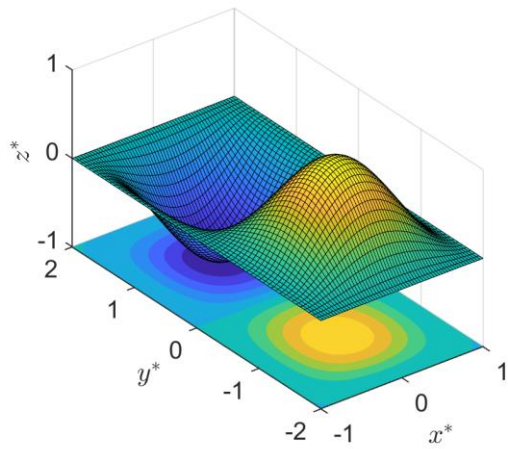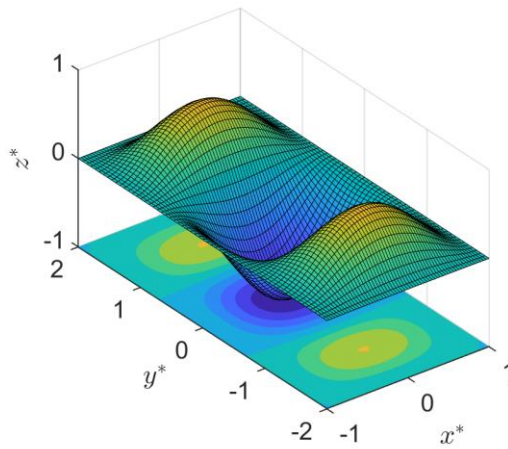
530 **FIG. 4.** Normalized mode shapes with completely clamped edges in a non-square tank: $b^* =$
531 $2, m^* = 0.001, L^* = 0.1, H^* = 1, \nu = 0.3$. (a). $\omega^* = 2.6628$ (S-A); (b). $\omega^* = 5.1360$ (S-S); (c). $\omega^* =$
532 7.6821 (A-S); (d). $\omega^* = 8.4637$(S-A); (e). $\omega^* = 9.2951$(A-A); (f). $\omega^* = 11.9837$ (A-S).

533

5. Principal Strain

535 The principal strain of the rectangular plate cover can be calculated as the eigenvalues
536 of the following strain tensor matrix

$$\boldsymbol{\varepsilon} = -\frac{h}{2}\begin{bmatrix} W_{xx} & W_{xy} \\ W_{xy} & W_{yy} \end{bmatrix}, \tag{34}$$

538 or the solution of $\det[\boldsymbol{\varepsilon} - \lambda \boldsymbol{I_2}] = 0$, where $\boldsymbol{I_2}$ is the identity matrix of size 2. It further
539 yields

$$\lambda_{1,2}(x, y, t) = -\frac{h \cos \omega t}{4}\left[w_{xx} + w_{yy} \pm \sqrt{(w_{xx} - w_{yy})^2 + 4w_{xy}^2}\right], \tag{35}$$

541 given that w is real and thus $W = \text{Re}\{w(x, y) \times e^{-i\omega t}\} = w \cos \omega t$. For each position
542 (x, y), the maximum of the principal values $\lambda_{max}(x, y)$ can be obtained as

543 $\max\left\{\left|\frac{\lambda_1}{\cos \omega t}\right|, \left|\frac{\lambda_2}{\cos \omega t}\right|\right\}$, or $\lambda_{max}(x, y) = \frac{h}{4}\left[|w_{xx} + w_{yy}| + \sqrt{(w_{xx} - w_{yy})^2 + 4w_{xy}^2}\right]$. A

544 similar procedure can be found in Ren et al.[26] for an upright circular cylindrical tank
545 with an elastic cover. In Fig. 5, we display the maximal principal strain at different
546 positions on the elastic cover with completely clamped edges in a non-square tank at
547 different natural modes corresponding to the cases shown in Fig. 4. From the figure, we
548 can observe that when the mode shape becomes more oscillatory, the maximum
549 principal strain tends to more oscillatory as well. For the clamped edge case, the peaks
550 of the maximum principal strain occur on the edge, which is consistent with the
551 observation in the rectangular channel[28].

(a)
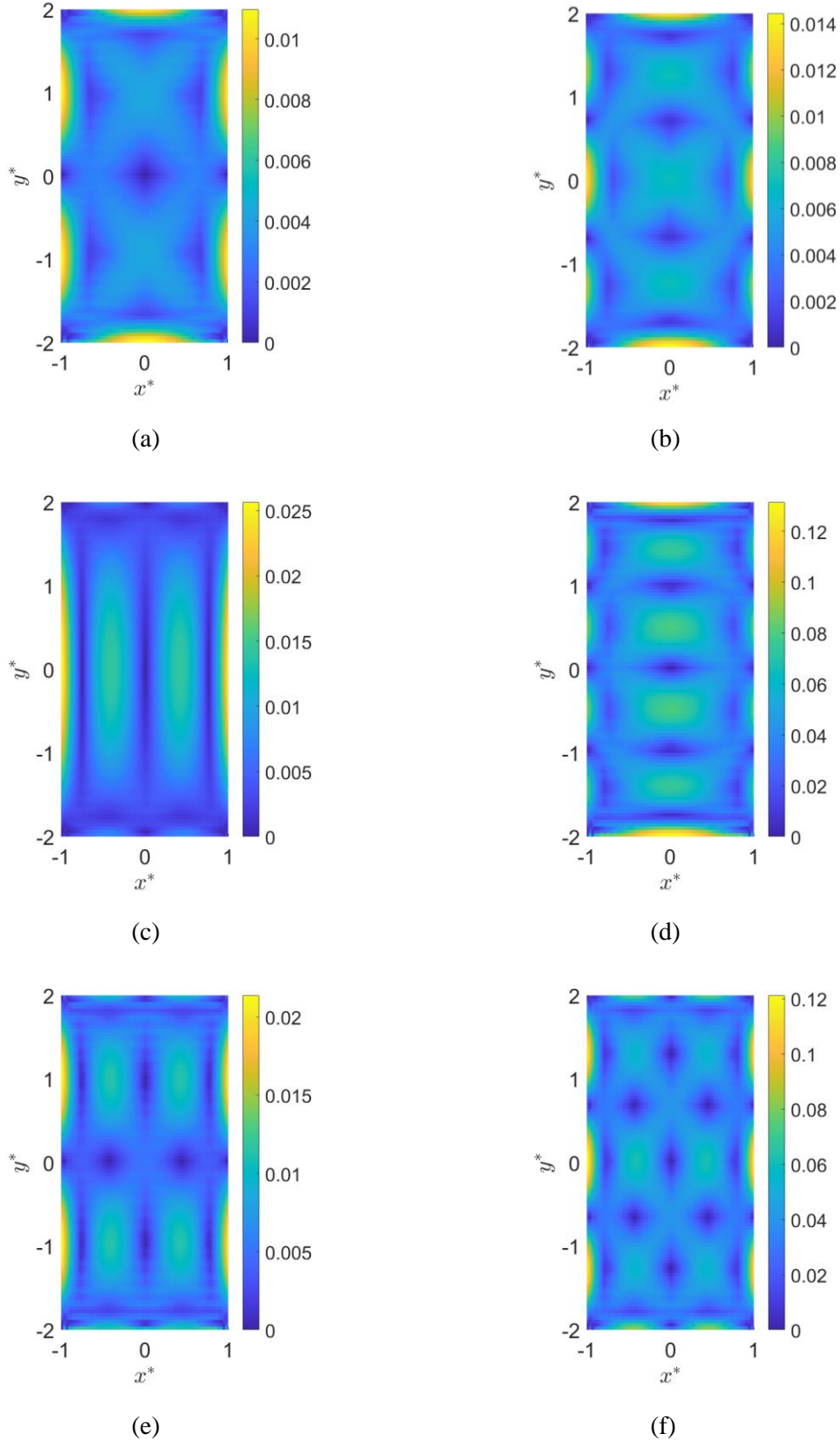
(b)

(c)

(d)

(e)

(f)

FIG. 5. Maximal principal strain distribution on the elastic cover with completely clamped edges (C-C-C-C): $b^* = 2, h^* = 0.001, m^* = 0.001, L^* = 0.1, H^* = 1, \nu = 0.3$. (a). $\omega^* = 2.6628$ (S-A) at $I_{01}^* = 1$; (b). $\omega^* = 5.1360$ (S-S) at $I_{02}^* = 1$; (c). $\omega^* = 7.6821$ (A-S) at $I_{10}^* = 1$; (d). $\omega^* = 8.4637$ (S-A) at $I_{01}^* = 1$; (e). $\omega^* = 9.2951$ (A-A) at $I_{11}^* = 1$; (f). $\omega^* = 11.9837$ (A-S) at $I_{10}^* = 1$.

6. Conclusions

An efficient solution scheme has been developed to investigate the coupled free vibrations of liquid in a three-dimensional rectangular container covered by an elastic cover. This scheme is applicable for any combinations of edge conditions. Examples are provided for the three most common ones, namely, clamped, free edge and simply supported.

When $\rho \to 0$, the results are not always identical to that when $\rho = 0$. This is due to the assumption of the incompressible liquid, which may not be valid as $\rho \to 0$. When the compressibility effect is included through replacing the Laplace equation with the wave equation, these two cases of $\rho \to 0$ and $\rho = 0$ become identical.

When the cover has the same edge type on its four sides, the entire coefficient matrix can be split into four independent block matrices, from which four groups of natural frequencies can be obtained. Correspondingly, the natural modes can be split into four mode groups which are uncoupled from each other, with mode shapes either symmetric (S) or antisymmetric (A) with respect to the longitudinal and transverse directions, respectively. For a square tank, the S-A and A-S modes share the same natural frequencies, and their mode shapes could be mutually converted through rotating the tank in clockwise or counter-clockwise direction by 90 degrees.

The effect of aspect ratios of the tank on natural frequencies is investigated through various b/l. It is observed that the elastic cover with completely clamped edges, the present results show a similar trend with those of a rectangular cover in vacuum. However, for the completely free or completely simply supported case, due to the effect of the tank walls and fluid, the trends will no longer be the same as those of a rectangular cover in vacuum.

591 For different natural modes in each mode group, it is observed that both the graphs of

592 mode shape and the maximum principal strain become more oscillatory with the

593 increase of natural frequencies. The peaks of the maximum principal strain occur at the

594 side walls for completely clamped edge case.

595

References

597 [1]B.W. Wilson, "Seiches", Adv. Hydrosci. 8, 1-94 (1972) doi: 10.1016/B978-0-12-021808-0.50006-1

598 [2]O.F. Rognebakke, O.M. Faltinsen, "Coupling of sloshing and ship motions", J. Ship Res. 47, 208-221
599 (2003) doi:10.5957/jsr.2003.47.3.208

600 [3]S. Wu, Y. Ju, "Numerical study of the boil-off gas (BOG) generation characteristics in a type C
601 independent liquefied natural gas (LNG) tank under sloshing excitation", Energy. 223, 120001 (2021)
602 doi: 10.1016/j.energy.2021.120001

603 [4]A.E. Veldman, J. Gerrits, R. Luppes, J.A. Helder, J.P.B. Vreeburg, "The numerical simulation of liquid
604 sloshing on board spacecraft," J. Comput. Phys. 224, 82-99 (2007) doi:10.1016/j.jcp.2006.12.020

605 [5]C. Farhat, E.K.Y. Chiu, D. Amsallem, J.S. Schotté, R. Ohayon, "Modeling of fuel sloshing and its
606 physical effects on flutter," AIAA J. 51, 2252-2265 (2013) doi:10.2514/1.J052299

607 [6]S.M. Longshaw, B.D. Rogers, "Automotive fuel cell sloshing under temporally and spatially varying
608 high acceleration using GPU-based Smoothed Particle Hydrodynamics (SPH)," Adv. Eng. Softw. 83,
609 31-44 (2015) doi: 10.1016/j.advengsoft.2015.01.008

610 [7]M.J. Smith, J.J. Kobine, F.A. Davidson, "Free and forced motion in an asymmetric liquid-column
611 oscillator," Proc. R. Soc. A. 464, 905-922 (2008) doi: 10.1098/rspa.2007.0375

612 [8]R.A. Ibrahim, "Liquid sloshing dynamics: theory and applications," Cambridge University Press,
613 Cambridge (2005)

614 [9]O.M. Faltinsen, A.N. Timokha, "Sloshing," Cambridge University Press, Cambridge (2009)

615 [10]H.N. Abramson, "The dynamic behavior of liquids in moving containers," Report SP 106, NASA,
616 (1966)

617 [11]G.X. Wu, Q.W. Ma, R. Eatock Taylor, "Numerical simulation of sloshing waves in a 3D tank based
618 on a finite element method," Appl. Ocean Res. 20, 337-355 (1998) doi:10.1016/S0141-1187(98)00030-
619 3

620 [12]O.M. Faltinsen, O.F. Rognebakke, A.N. Timokha, "Resonant three-dimensional nonlinear sloshing in
621 a square-base basin", J. Fluid Mech. 487, 1-42 (2003) doi:10.1017/S0022112003004816

622 [13]D. Liu, P. Lin, "A numerical study of three-dimensional liquid sloshing in tanks," J. of Comput.
623 Phys. 227, 3921-3939 (2008) doi:10.1016/j.jcp.2007.12.006

624 [14]P.A. Caron, M.A. Cruchaga and A. E. Larreteguy, "Study of 3D sloshing in a vertical cylindrical
625 tank," Phys. Fluids 30, 082112 (2018) doi:10.1063/1.5043366

[15]J. Núñez Aedo, M. Cruchaga, and E. Castillo del Barrio, "Study on the dependence with the filling level of the sloshing wave pattern in a rectangular tank," Phys. Fluids 32, 012101 (2020) doi: 10.1063/1.5133420

[16]C. Zhang, X. Sun, P. Wang, L. Chen, and D. Ning, "Hydrodynamics of a floating liquid-tank barge adjacent to fixed structure in beam waves," Phys. Fluids 34, 047114 (2022) doi:10.1063/5.0089127

[17]N.G. Kuznetsov, O.V. Motygin, "Sloshing in vertical cylinders with circular walls: The effect of radial baffles," Phys. Fluids 33, 102106 (2021) doi:10.1063/5.0064549

[18]E. Hernández, D. Santamarina, "Active control of sloshing in containers with elastic baffle plates," Int. J. Numer. Methods Eng. 91, 604-621 (2012) doi: 10.1002/nme.4283

[19]S.M. Hasheminejad, M.M. Mohammadi, A. Jamalpoor, "Hydroelastic modeling and active control of transient sloshing in a three dimensional rectangular floating roof tank," J. Sound Vib. 470, 115146 (2020) doi: 10.1016/j.jsv.2019.115146

[20]Y. Xie, X. Zhao, "Sloshing suppression with active controlled baffles through deep reinforcement learning–expert demonstrations–behavior cloning process," Phys. Fluids, 33, 017115. (2021) doi:10.1063/5.0037334

[21]H.F. Bauer, "Coupled frequencies of a liquid in a circular cylindrical container with elastic liquid surface cover," J. Sound Vib. 180, 689-704 (1995) doi: 10.1006/jsvi.1995.0109

[22]W. Parasil, and N. Watanabe, "Nonlinear dynamic analysis of the interaction between a two-dimensional rubberlike membrane and a liquid in a rectangular tank," Aerospace Science and Technology 56, 212-222 (2016) doi: 10.1016/j.ast.2016.07.013

[23]H.F. Bauer, K. Komatsu, "Coupled frequencies of a frictionless liquid in a circular cylindrical tank with an elastic partial surface cover," J. Sound Vib. 230, 1147-1163 (2000) doi: 10.1006/jsvi.1999.2662

[24]Y.W. Kim, Y.S. Lee, "Coupled vibration analysis of liquid-filled rigid cylindrical storage tank with an annular plate cover," J. Sound Vib. 279, 217-235 (2005) doi:10.1016/j.jsv.2003.10.032

[25]M. Amabili, "Vibrations of circular plates resting on a sloshing liquid: solution of the fully coupled problem," J. Sound Vib. 245 (2001) 261-283. doi: 10.1006/jsvi.2000.3560

[26]K. Ren, G.X. Wu, Z.F. Li, "Natural modes of liquid sloshing in a cylindrical container with an elastic cover," J. Sound Vib. (2021). doi: 10.1016/j.jsv.2021.116390

[27]T. Matsui, "Sloshing in a cylindrical liquid storage tank with a single-deck type floating roof under seismic excitation," ASME. J. Pressure Vessel Technol. 131, 021303 (2009) doi: 10.1115/1.3062939

[28]K. Ren, G.X. Wu, Z.F. Li, "Hydroelastic waves propagating in an ice-covered channel," J. Fluid Mech. 886, A18 (2020) doi:10.1017/jfm.2019.1042

[29]S.P. Timoshenko, S. Woinowsky-Krieger, "Theory of plates and shells," McGraw-Hill, New York (1959)

660   [30]A.W. Leissa, "The free vibration of rectangular plate," J. Sound Vib. 31, 257-293 (1973) doi:
661   10.1016/S0022-460X(73)80371-2

662   [31]W. L. Li, X. Zhang, J. Du, Z. Liu, "An exact series solution for the transverse vibration of rectangular
663   plates with general elastic boundary supports," J. Sound Vib. 321, 254-269 (2009) doi:
664   10.1016/j.jsv.2008.09.035

665

Acknowledgment

670

Appendix A. Linear equations for completely clamped edges case

From $w(x = -l) = 0$:

$$\sum_{i=1}^{4} \underbrace{\sum_{m=0}^{\infty} \left(\mu_m^{(i)} S_{mn} + \beta_{mn}^{(i)} \right) T_{mn}}_{A_{1i}} d_n^{(i)} = -\sum_{m=0}^{\infty} \sum_{i=1}^{4} \left(\mu_n^{(i)} S_{mn} + \alpha_{mn}^{(i)} \right) T_{mn} c_m^{(i)},$$

$$(n = 0,1,2,\dots) \qquad (A.1)$$

From $w(x = l) = 0$:

$$\sum_{i=1}^{4} \underbrace{\sum_{m=0}^{\infty} \left(\mu_m^{(i)} S_{mn} + \beta_{mn}^{(i)} \right) T_{mn} (-1)^m}_{A_{2i}} d_n^{(i)}$$

$$= -\sum_{m=0}^{\infty} \sum_{i=1}^{4} \left(\mu_n^{(i)} S_{mn} + \alpha_{mn}^{(i)} \right) T_{mn} (-1)^m c_m^{(i)},$$

$$(n = 0,1,2,\dots) \qquad (A.2)$$

From $w(y = -b) = 0$:

$$\sum_{i=1}^{4} \underbrace{\sum_{n=0}^{\infty} \left(\mu_n^{(i)} S_{mn} + \alpha_{mn}^{(i)} \right) T_{mn}}_{B_{1i}} c_m^{(i)} = -\sum_{n=0}^{\infty} \sum_{i=1}^{4} \left(\mu_m^{(i)} S_{mn} + \beta_{mn}^{(i)} \right) T_{mn} d_n^{(i)},$$

681 $\qquad\qquad\qquad\qquad\qquad\qquad (m = 0,1,2, \dots)$ $\qquad$ (A. 3)

682 From $w(y = b) = 0$:

683 $$\sum_{i=1}^{4} \underbrace{\sum_{n=0}^{\infty} \left(\mu_n^{(i)} S_{mn} + \alpha_{mn}^{(i)}\right) T_{mn} (-1)^n}_{B_{2i}} c_m^{(i)} = -\sum_{n=0}^{\infty} \sum_{i=1}^{4} \left(\mu_m^{(i)} S_{mn} + \beta_{mn}^{(i)}\right) T_{mn}(-1)^n d_n^{(i)},$$

684 $\qquad\qquad\qquad\qquad\qquad\qquad (m = 0,1,2, \dots)$ $\qquad$ (A. 4)

685 From $w_x(x = -l) = 0$:

686 $$\sum_{i=1}^{4} i \times (-1)^{i-1} \times d_n^{(i)} = 0, \qquad\qquad (n = 0,1,2, \dots) \qquad (A. 5)$$

687 From $w_x(x = l) = 0$:

688 $$\sum_{i=1}^{4} i \times d_n^{(i)} = 0, \qquad\qquad\qquad (n = 0,1,2, \dots) \qquad (A. 6)$$

689 From $w_y(y = -b) = 0$:

690 $$\sum_{i=1}^{4} i \times (-1)^{i-1} \times c_m^{(i)} = 0, \qquad\qquad (m = 0,1,2, \dots) \qquad (A. 7)$$

691 From $w_y(y = b) = 0$:

692 $$\sum_{i=1}^{4} i \times c_m^{(i)} = 0 . \qquad\qquad\qquad (m = 0,1,2, \dots) \qquad (A. 8)$$

693 Through $(A. 1) \pm (A. 2)$, $(A. 5) \pm (A. 6)$, and using $\mu_{2n}^{(1)} = \mu_{2n}^{(3)} = 0$ and $\mu_{2n+1}^{(2)} =$

694 $\mu_{2n+1}^{(4)} = 0$, we can obtain

695 $$d_n^{(1)} = \frac{Y_1}{\left(2A_{11} - \frac{2}{3} A_{13}\right)}; \, d_n^{(3)} = -\frac{d_n^{(1)}}{3};$$

696 $$d_n^{(2)} = \frac{Y_2}{(2A_{12} - A_{14})}; \, d_n^{(4)} = -\frac{d_n^{(2)}}{2};$$

697   where Y_1 has only c_{2m+1} terms and Y_2 has only c_{2m} terms.

698

699   Through (A. 3) $\pm$ (A. 4), (A. 7) $\pm$ (A. 8), we can write c_m in terms of d_n in a similar

700   way as

701
$$c_m^{(1)} = \frac{X_1}{\left(2B_{11} - \frac{2}{3}B_{13}\right)}; \quad c_m^{(3)} = -\frac{c_m^{(1)}}{3};$$

702
$$c_m^{(2)} = \frac{X_2}{(2B_{12} - B_{14})}; \quad c_m^{(4)} = -\frac{c_m^{(2)}}{2};$$

703   where X_1 has only d_{2n+1} terms and X_2 has only d_{2n} terms. Then, we put d_n into X_1 and

704   X_2 , and we can split all the unknowns of c_m into four groups, namely

705    $c_{2m}^{(2i)}, c_{2m}^{(2i-1)}, c_{2m+1}^{(2i)}$ and $c_{2m+1}^{(2i-1)}$ $(i = 1,2; m = 0,1,2 \dots)$. Similarly, we can also split

706    $d_n^{(i)}$ into four groups as $d_{2n}^{(2i)}, d_{2n}^{(2i-1)}, d_{2n+1}^{(2i)}$ and $d_{2n+1}^{(2i-1)}$ $(i = 1,2; n = 0,1,2 \dots)$. Then,

707   the unknowns can be split into four fully independent groups, namely: (a). $c_{2m}^{(2i)}, d_{2n}^{(2i)}$;

708   (b). $c_{2m}^{(2i-1)}, d_{2n+1}^{(2i)}$; (c). $c_{2m+1}^{(2i)}, d_{2n}^{(2i-1)}$; and (d). $c_{2m+1}^{(2i-1)}, d_{2n+1}^{(2i-1)}$, while within each group,

709   the unknowns are coupled.

710

711   **Appendix B. Linear equations for completely free edges**

712   From $\left[\frac{\partial^2 w}{\partial x^2} + v\frac{\partial^2 w}{\partial y^2}\right]_{x=-l} = 0$:

713
$$-\sum_{m=0}^{\infty}\sum_{i=1}^{4}\left\{(a_m^2 + vb_n^2) \times \frac{\alpha_{mn}^{(i)}k_{mn}\tanh k_{mn}H - \rho\omega^2\mu_n^{(i)}}{k_{mn}S_{mn}\tanh k_{mn}H + \rho\omega^2}\right.$$

714
$$\left. + \left(a_m^2\mu_n^{(i)} - \frac{v(i-1)i\,\mu_n^{(i-2)}}{b^2}\right)\right\}c_m^{(i)}$$

715
$$-\sum_{i=1}^{4}\left\{\sum_{m=0}^{\infty}(a_m^2 + vb_n^2) \times \frac{\beta_{mn}^{(i)}k_{mn}\tanh k_{mn}H - \rho\omega^2\mu_m^{(i)}}{k_{mn}S_{mn}\tanh k_{mn}H + \rho\omega^2}\right.$$

716
$$\left. + (-1)^{i+1}\left(-vb_n^2 + \frac{(i-1)i}{l^2}\right)\right\}d_n^{(i)} = 0 \qquad (n = 0,1,2, \dots) \quad (\text{B. 1})$$

717   From $\left[\dfrac{\partial^2 w}{\partial x^2} + \nu \dfrac{\partial^2 w}{\partial y^2}\right]_{x=l} = 0$:

718

$$-\sum_{m=0}^{\infty}\sum_{i=1}^{4}(-1)^m\left\{(a_m^2+\nu b_n^2)\times\frac{\alpha_{mn}^{(i)}k_{mn}\tanh k_{mn}H-\rho\omega^2\mu_n^{(i)}}{k_{mn}S_{mn}\tanh k_{mn}H+\rho\omega^2}\right.$$

719

$$\left.+\left(a_m^2\mu_n^{(i)}-\frac{\nu(i-1)i\,\mu_n^{(i-2)}}{b^2}\right)\right\}c_m^{(i)}$$

720

$$-\sum_{i=1}^{4}\left\{\sum_{m=0}^{\infty}(a_m^2+\nu b_n^2)(-1)^m\times\frac{\beta_{mn}^{(i)}k_{mn}\tanh k_{mn}H-\rho\omega^2\mu_m^{(i)}}{k_{mn}S_{mn}\tanh k_{mn}H+\rho\omega^2}\right.$$

721

$$\left.+\left(\nu b_n^2-\frac{(i-1)i}{l^2}\right)\right\}d_n^{(i)}=0 \qquad\qquad (n=0,1,2,\dots)\quad (\text{B}.2)$$

722   From $\left[\dfrac{\partial^2 w}{\partial y^2} + \nu \dfrac{\partial^2 w}{\partial x^2}\right]_{y=-b} = 0$:

723

$$-\sum_{i=1}^{4}\left\{\sum_{n=0}^{\infty}(\nu a_m^2+b_n^2)\times\frac{\alpha_{mn}^{(i)}k_{mn}\tanh k_{mn}H-\rho\omega^2\mu_n^{(i)}}{k_{mn}S_{mn}\tanh k_{mn}H+\rho\omega^2}\right.$$

724

$$\left.+(-1)^i\left(\nu a_m^2-\frac{(i-1)i}{b^2}\right)\right\}c_m^{(i)}$$

725

$$-\sum_{n=0}^{\infty}\sum_{i=1}^{4}\left\{(\nu a_m^2+b_n^2)\times\frac{\beta_{mn}^{(i)}k_{mn}\tanh k_{mn}H-\rho\omega^2\mu_m^{(i)}}{k_{mn}S_{mn}\tanh k_{mn}H+\rho\omega^2}\right.$$

726

$$\left.+\left(b_n^2\mu_m^{(i)}-\frac{\nu(i-1)i\,\mu_m^{(i-2)}}{l^2}\right)\right\}d_n^{(i)}=0 \qquad (m=0,1,2,\dots)\quad (\text{B}.3)$$

727   From $\left[\dfrac{\partial^2 w}{\partial y^2} + \nu \dfrac{\partial^2 w}{\partial x^2}\right]_{y=b} = 0$:

728

$$-\sum_{i=1}^{4}\left\{\sum_{n=0}^{\infty}(\nu a_m^2+b_n^2)(-1)^n\times\frac{\alpha_{mn}^{(i)}k_{mn}\tanh k_{mn}H-\rho\omega^2\mu_n^{(i)}}{k_{mn}S_{mn}\tanh k_{mn}H+\rho\omega^2}\right.$$

729

$$\left.+\left(\nu a_m^2-\frac{(i-1)i}{b^2}\right)\right\}c_m^{(i)}$$

730

$$-\sum_{n=0}^{\infty}\sum_{i=1}^{4}(-1)^n\left\{(\nu a_m^2+b_n^2)\times\frac{\beta_{mn}^{(i)}k_{mn}\tanh k_{mn}H-\rho\omega^2\mu_m^{(i)}}{k_{mn}S_{mn}\tanh k_{mn}H+\rho\omega^2}\right.$$

731

$$\left.+\left(b_n^2\mu_m^{(i)}-\frac{\nu(i-1)i\,\mu_m^{(i-2)}}{l^2}\right)\right\}d_n^{(i)}=0 \qquad (m=0,1,2,\dots)\quad (\text{B}.4)$$

732   From $\left[\frac{\partial^3 w}{\partial x^3} + (2-v)\frac{\partial^3 w}{\partial x \partial y^2}\right]_{x=-l} = 0$:

733    $$\sum_{i=1}^{4}\left(\frac{(2-v)b_n^2}{l} \times (-1)^i \times i + \frac{6\delta_{i3}}{l^3} - \frac{24\delta_{i4}}{l^3}\right) d_n^{(i)} = 0 \qquad (n = 0,1,2,\dots) \quad (\text{B.}5)$$

734   From $\left[\frac{\partial^3 w}{\partial x^3} + (2-v)\frac{\partial^3 w}{\partial x \partial y^2}\right]_{x=l} = 0$:

735    $$\sum_{i=1}^{4}\left(-\frac{(2-v)b_n^2}{l} \times i + \frac{6\delta_{i3}}{l^3} + \frac{24\delta_{i4}}{l^3}\right) d_n^{(i)} = 0 \qquad (n = 0,1,2,\dots) \quad (\text{B.}6)$$

736   From $\left[\frac{\partial^3 w}{\partial y^3} + (2-v)\frac{\partial^3 w}{\partial y \partial x^2}\right]_{y=-b} = 0$:

737    $$\sum_{i=1}^{4}\left(\frac{(2-v)a_m^2}{b} \times (-1)^i \times i + \frac{6\delta_{i3}}{b^3} - \frac{24\delta_{i4}}{b^3}\right) c_m^{(i)} = 0 \qquad (m = 0,1,2,\dots) \quad (\text{B.}7)$$

738   From $\left[\frac{\partial^3 w}{\partial y^3} + (2-v)\frac{\partial^3 w}{\partial y \partial x^2}\right]_{y=b} = 0$:

739    $$\sum_{i=1}^{4}\left(-\frac{(2-v)a_m^2}{b} \times i + \frac{6\delta_{i3}}{b^3} + \frac{24\delta_{i4}}{b^3}\right) c_m^{(i)} = 0 \qquad (m = 0,1,2,\dots) \quad (\text{B.}8)$$